Combustion and Flame 244 (2022) 112276

Contents lists available at ScienceDirect

Combustion and Flame

journal homepage: www.elsevier.com/locate/combustflame

Stretched vortex layer flamelet

William A. Sirignano

Department of Mechanical and Aerospace Engineering, University of California, Irvine CA 92697, USA

ARTICLE INFO

Article history:
Received 25 May 2022
Revised 20 June 2022
Accepted 21 June 2022

ABSTRACT

A new sub-grid flamelet model is developed based on a steady-state, viscous vortex layer with an imposed compressive strain orthogonal to both the vorticity and the shear force. The imposed normal strain results in the stretching of the vorticity in the direction orthogonal to the plane of the shear strain. The model has certain special features. (i) Non-premixed flames, premixed flames, or multi-branched flame structures are determined rather than prescribed. (ii) Three components of velocity exist although the flamelet model is two-dimensional. (iii) The effect of variable density is addressed in the flamelet model. The vortex-layer configuration distinguishes this model from recent models by this author that address flames in other practical and ubiquitous vortical structures: tube-like stretched vortices or vortices stretched in two directions. Thereby, the model collection available for application to vortical configurations found in turbulent combustion is increased. Solutions to the Navier-Stokes equations and the associated scalar equations governing the flamelet model are obtained without the boundary-layer approximation and demonstrate the impact of the new features of the model. The shear strain and vorticity are found not to affect the scalar profiles, mixing and burning rates, or the two velocity components orthogonal to the shear force; only the velocity parallel to the shear force is affected. The compressive strain rate is the influential constraint affecting the scalars and the other two velocity components. However, the vorticity is strongly affected by the scalar profiles. The relation to classical concepts for incompressible flow is discussed.

© 2022 The Combustion Institute. Published by Elsevier Inc. All rights reserved.

1. Introduction

The major method for energy conversion for high levels of mechanical power and heating continues to be combustion with high mass fluxes. Inherently, the high mass-flow rate involves turbulent flow. Consequently, many physical length and time scales emerge and present challenges for both computational and experimental analyses. Large-eddy simulations (LES) are employed for computations where the smallest scales cannot be resolved. The smaller scales are filtered via integration over a window size commensurate with the computational mesh size, thereby allowing affordable computations. Consequently, the essential, rate-controlling, physical and chemical processes that occur on the smaller scales than the filter size must be described by closure models. Flamelet models provide a method of closure with a very explicit representation of the key physics.

The flamelet models should handle multi-species, multi-step oxidation kinetics without requiring small time steps during the solution of the resolved-scale fluid dynamics. Thus, savings of computational resources can be huge compared to direct numerical simulation. The focus here is on the types of turbulent flames found in the shear-driven flows of practical combustors. Thereby, we address flamelets as originally described by Williams [1], namely "highly sheared small diffusion flamelets" and "forming a turbulent flame brush which appears on the average to fill" the flow domain.

There is need to understand the laminar mixing and combustion that commonly occur within the smallest turbulent eddies. These laminar flamelet sub-domains experience significant strain of all types: shear, tensile, and compressive. Notable works exist for either counterflows with only normal strain or simple vortex structures in two-dimensions or axisymmetry and often with a constant-density approximation. See Linan [2], Marble [3], Karagozian and Marble [4]), Cetegen and Sirignano [5,6], Peters [7], and Pierce and Moin [8]. An interesting review of the early flamelet theory is given by Williams [9]. A more recent review of premixed flamelets is provided by van Oijens et al. [10] Flamelet studies have focused on either premixed or nonpremixed flames; a unifying approach to premixed, nonpremixed, and multi-branched flames is needed.

Many flamelet studies have not directly considered vorticity interaction with the flamelet [2,7–9,11]. The two-dimensional planar or axisymmetric counterflow configuration has become a founda-

E-mail address: sirignan@uci.edu

https://doi.org/10.1016/j.combustflame.2022.112276
0010-2180/© 2022 The Combustion Institute. Published by Elsevier Inc. All rights reserved.

tion for flamelet model. Local conversion to a coordinate system based on the principal strain-rate directions can provide the counterflow configuration in a general flow. Furthermore, the quasi-steady counterflow can be analyzed by ordinary differential equations because the dependence on the transverse coordinate is either constant or linear, depending on the variable. The mixture fraction has been used widely as an independent variable to display non-premixed flamelet scalar variations; this cannot be useful for premixed flames if mass diffusivity is identical for all species. Sirignano [12] has shown that any conserved scalar can serve well as an independent variable to present scalar results for non-premixed and multi-branched flamelets.

Experiments and asymptotic analysis by Hamins et al. [13] show that a partially premixed fuel-lean flame and a diffusion flame can co-exist in a counterflow with opposing streams of heptane vapor and methane-oxygen-nitrogen mixture. Thus, a need exists for flamelet theory to address both premixed and non-premixed flames. Recently, Rajamanickam et al. [14] provided an interesting three-dimensional triple-flame analysis, describing the effect of imposed normal strain on a multibranched flame. They did not consider shear strain, but it was followed by the work of Sirignano [15] where both shear strain and normal strain were considered.

The classical counterflow treatment [2,7] has two opposing streams, fuel or fuel plus a chemically inert gas and oxidizer or oxidizer plus an inert gas. They considered uniform density. That critical assumption was relaxed [12,15,16] for reacting flows and heated flows. Sirignano [12,15] with one-step kinetics and Lopez et al. [17] with detailed kinetics address situations where the inflowing streams consist of a combustible mixture of fuel and oxidizer, thereby allowing another flame or two besides the simple diffusion flame to co-exist. A recent counterflow analysis [12] shows the various permissible flame configurations pertaining to the specific compositions of the inflowing streams: (i) three flames including fuel-lean partially premixed, nonpremixed (i.e., diffusion-controlled), and fuel-rich partially premixed; (ii) nonpremixed and fuel-rich partially premixed; (iii) fuel-lean partially premixed and nonpremixed; (iv) nonpremixed; and (v) premixed. The counterflow analysis was extended [17] to consider detailed kinetics for methane-oxygen detailed chemical kinetics and confirmed that combinations of premixed and non-premixed flames could exist in a multi-flame counterflow. Note that Rajamanickam et al. [14] and Lopez et al. [17] considered multibranched flames without consideration of the shear strain and vorticity. Ramaekers et al. [18] considered premixed flames and diffusion flames without consideration of multibranched flames or vorticity.

The effects of both normal strain rate and shear strain rate should be determined. Mixing and combustion in three-dimensional flows needs to be studied with imposed normal strain and shear strain and therein imposed vorticity.

Generally, for flows with zero or modest values for velocity divergence, one principal strain rate γ locally will be compressive (corresponding to inflow in a counterflow configuration), another principal strain rate α will be tensile (also named extensional and corresponding to outflow), and the third can be either extensional or compressive and will have an intermediate strain rate β of lower magnitude than the other like strain rate. Specifically, $\alpha > \beta > \gamma$, $\alpha > 0$, $\gamma < 0$, and, for incompressible flow, $\alpha + \beta + \gamma = 0$. With $\beta < 0$, there is inflow from two directions with outflow in one direction; a contracting jet flow occurs locally. Conversely, with $\beta > 0$, there is outflow in two directions and inflow in one direction; i.e., a counterflow.

Direct numerical simulations (DNS) for incompressible flows give helpful results. Ashurst et al. [19] and Nomura and Eghobashi [20] both compared a case of homogeneous sheared turbulence with a case of isotropic turbulence. The vorticity alignment with the intermediate strain direction is found to be most probable in both cases but especially in the case with shear. The intermediate strain rate is most likely to be extensive (positive) implying a counterflow configuration. Elghobashi and Nomura [21] studied reacting flow and show that in regions of exothermic reaction and variable density, alignment of the vorticity with the most tensile strain direction can occur. Several researchers [19–23] indicate that the scalar gradient and the direction of compressive strain are aligned. Furthermore, there is agreement that the most common intermittent vortex structures in regions of high strain rate are sheets or ribbons rather than tubes.

Based on those understandings concerning vector orientations, flamelet theory was extended [15] in a second significant aspect beyond the inclusion of both premixed and non-premixed flame structures; namely, a model was created of a three-dimensional field with both shear and normal strains. The three-dimensional problem is reduced to a two-dimensional form and then, for the counterflow or mixing-layer flow, to a one-dimensional similar form. The system of ordinary differential equations (ODEs) is presented for the thermo-chemical variables and the velocity components. Similarly, Sirignano [24,25] was able to consider three-dimensional problems, with both shear strain (or equivalently vorticity) and normal strain, and reduce them to one-dimensional descriptions, which were readily solvable by numerical analysis. It is well known that different vortical structures can exist in turbulent flows. Flamelet models are needed for the various different vortical structures. Flamelet configurations have recently been examined with the vortical flow field stretched in two directions (one parallel to the vorticity and the other orthogonal) [24] and with a stretched-vortex-tube structure with inward swirl [25]. These new findings improve the foundations for flamelet theory and its use in sub-grid modeling for turbulent combustion. In the next section, another new configuration to be studied is explained.

In view of the needed improvements, the aim here is to develop another flamelet model that is inspired by the incompressible flow analysis for a stretched vortex layer by Burgers [26–28]. A relevant and interesting flow-field configuration with three components of velocity, shear strain, and normal strain can again be reduced to a one-dimensional analysis. The new flamelet model discussed in the next section will retain certain desirable features; specifically, the model (i) determines rather than prescribes the existence of non-premixed flames, premixed flames, or multi-branched flame structures; (ii) determines directly the effect of shear strain and vorticity on the flames; and (iii) considers the effect of variable density. The analysis uses one-step kinetics, uniform Fickian diffusion for all species, and simplified thermophysical properties to avoid complications in this initial study; however, a clear template is established for the employment of multi-step kinetics.

2. Flamelet analysis

We formulate the problem in a quasi-steady three-dimensional form. The following alignments will be assumed. The direction of major compressive principal strain is orthogonal to the vorticity vector direction. Specifically, the intermediate principal strain direction is aligned with the vorticity while the scalar gradient aligns with the principal compressive strain direction. These assumptions are consistent with the statistical findings [21]. Variable density with low Mach number will be considered. Both reacting and non-reacting flows can be studied but here the emphasis will be on reacting flow. Our analysis considers a steady, spatially developing shear layer in the x-direction with a two-dimensional imposed strain in the y,z plane. See the sketch provided in Fig. 1 to obtain a qualitative understanding of the flow field. The imposed strain can affect the growth of a spatially-developing shear-layer width with downstream distance. In principle, if the imposed strain rate is constant with x, an asymptote should be reached downstream

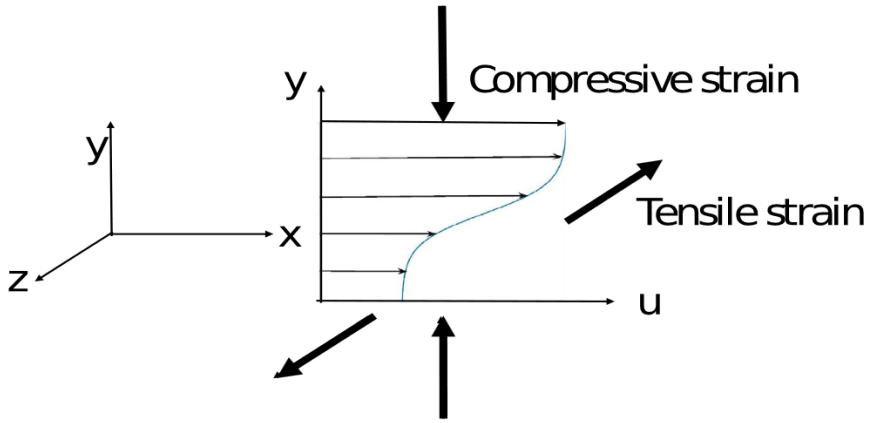

Fig. 1. Sketch of mixing-layer flow in the x, y plane with imposed counterflow presenting compressive strain in the y-direction and tensile (extensional) strain in the z-direction.

where layer thickness becomes constant. This expectation is consistent with recent unpublished findings by Palafoutas and Sirignano [29]. It also relates to the classical study [26]. In this work, the focus will be on a developed reacting shear layer with three components of velocity but no variation in the major flow direction (i.e., the x-direction).

The incompressible velocity field defined by the Burgers stretched vortex sheet has u_x, u_y, and u_z as the velocity components. The imposed normal strain rate $S > 0$, kinematic viscosity ν, and free stream velocity magnitude U are taken as positive constants. As $y \to \infty$, $u_x(x, y, z, t) \to U$, $\partial u_y/\partial y \to -S$, and $\partial u_z/\partial z \to S$. And, as $y \to -\infty$, $u_x(x, y, z, t) \to -U$, $\partial u_y/\partial y \to -S$, and $\partial u_z/\partial z \to S$. Then, the steady-state solution is found for the velocity components and the vorticity ω_z whereby

$$u_x = UErf\Big(\sqrt{\frac{S}{2\nu}}y\Big) \quad ; \quad u_y = -Sy \quad ; \quad u_z = Sz$$

where Erf is the error function and

$$\omega_z = -\frac{\partial u_x}{\partial y} = -U\sqrt{\frac{S}{2\pi\nu}}exp\Big(-\frac{Sy^2}{2\nu}\Big).$$

This description gives an exact steady-state solution to the incompressible Navier-Stokes equations. Although the sheet is being stretched in the z direction, diffusion of momentum and vorticity in the y direction allows a balance with advection in the y direction that results in a steady solution. Figure 1 would match the mathematical description if the inflection point for the u curve translated to $y = 0$ to match the error function.

The analysis in this reacting-flow paper relates to some interesting classical work on temporal, viscous, incompressible vortex layers and vortex tubes subject to normal strain. A finding in those classical studies was that a balance between the diffusion and advection of vorticity could be achieved. Burgers [30], followed by Rott [31], examined the axisymmetric behavior of a stretched vortex tube for incompressible flow. The stretching (extensive or tensile strain) in the direction aligned with the vorticity vector resulted in an inward swirling motion. The steady-state solution of the Navier-Stokes equation (known as Burgers stretched vortex tube) requires a matching of vorticity strength and viscosity such that radially outward diffusion of vorticity and radially inward advection of vorticity are in balance. The two-dimensional analog of the stretched vortex tube involves a viscous shear layer, which is simultaneously a vortex layer, subject to normal compressive strain in a direction orthogonal to the shear-layer stream direction and with the associated tensile strain aligned with the vortex vector. The solution of the steady-state configuration for this vortex layer has been attributed to unpublished work presented in lectures by Burgers [26]. The two-dimensional analog is also mentioned without attribution by Batchelor [27] where this layer is described as a vortex sheet. Neu [32] refers to this two-dimensional layer as the "stretched Burgers vortex sheet". Note that, in contrast, the description "vortex sheet" for an inviscid flow implies a mathematical discontinuity in velocity and a vortex sheet of zero thickness [33].

1984 was a productive year in the mathematical study of vortices. The vortex-tube analysis was developed further [28] but without the radial symmetry, e.g. oval shapes. For an elongated shape, a resemblance emerges with Burgers stretched vortex sheet. The stability of the axisymmetric Burgers vortex was examined. Neu [32] works with Burgers stretched vortex sheet showing that, for sufficient vortex strength (or insufficient imposed strain rate), it becomes unstable leading to the periodic array of rolled-up concentrated vortices with stretched braids. Corcos and co-workers have three papers on the general subject of the temporal viscous layer using deterministic modeling. Corcos and Sherman [34] address stability of a purely two-dimensional viscous vortex sheet without describing it as Burgers stretched vortex sheet. The roll-up of the two-dimensional flow is examined. Corcos and Lin [35] study the stability under three-dimensional perturbations. Lin and Corcos [36] study the phenomenon further exploring streamwise vorticity. An implication for flamelet theory is that a vortical layer or sheet can become unstable through the roll-up mechanism leading to larger vortex-tube structures. The general consensus from direct numerical simulations and experimental studies is that sheet-like (and ribbon-like) structures are more common than tube-like (and line-like) structures; however, both types can exist [21,37].

Based on existing knowledge for incompressible flow, we assume stretched-vortex-layers with variable density will have similar qualitative features. Namely, there will be a domain for strain rate, vortex strength, and layer length where a stable layer can exist. Therein, a need for a new flamelet model exists.

2.1. Governing equations

The governing equations for unsteady 3D flow can be written with $u_i = u, v, w$; $x_i = x, y, z$. The quantities $p, \rho, h, h_m, Y_m, \dot{\omega}, \mu, \lambda, D$, and c_p are pressure, density, specific enthalpy, heat of formation of species m, mass fraction of species m, chemical reaction rate of species m, dynamic viscosity, thermal conductivity, mass diffusivity, and specific heat, respectively. Furthermore, τ_{ij} is the viscous stress tensor and the Lewis number

$Le \equiv \lambda/(\rho D c_p)$.

$$\frac{\partial \rho}{\partial t} + \frac{\partial (\rho u_j)}{\partial x_j} = 0 \tag{1}$$

$$\rho \frac{\partial u_i}{\partial t} + \rho u_j \frac{\partial u_i}{\partial x_j} + \frac{\partial p}{\partial x_i} = \frac{\partial \tau_{ij}}{\partial x_j} \tag{2}$$

where, following the Stokes hypothesis for a Newtonian fluid,

$$\tau_{ij} = \mu \left[\frac{\partial u_i}{\partial x_j} + \frac{\partial u_j}{\partial x_i} - \frac{2}{3}\delta_{ij} \frac{\partial u_k}{\partial x_k} \right] \tag{3}$$

$$\rho \frac{\partial h}{\partial t} + \rho u_j \frac{\partial h}{\partial x_j} - \frac{\partial p}{\partial t} - u_j \frac{\partial p}{\partial x_j} = \frac{\partial}{\partial x_j}\left(\frac{\lambda}{c_p} \frac{\partial h}{\partial x_j} \right) + \frac{\partial}{\partial x_j}\left(\rho D (1 - Le) \Sigma_{m=1}^{N} h_m \frac{\partial Y_m}{\partial x_j} \right) - \rho \Sigma_{m=1}^{N} h_{f,m} \dot{\omega}_m + \tau_{ij} \frac{\partial u_i}{\partial x_j} \tag{4}$$

$$\rho \frac{\partial Y_m}{\partial t} + \rho u_j \frac{\partial Y_m}{\partial x_j} = \frac{\partial}{\partial x_j}\left(\rho D \frac{\partial Y_m}{\partial x_j} \right) + \rho \dot{\omega}_m \ ; \quad m = 1, 2, \ldots, N \tag{5}$$

Eqs. (1) through (5) together with the calorically-perfect-gas equation of state and the relations describing fluid physico-chemical properties give a complete description of behavior.

Here, we define the non-dimensional Prandtl, Schmidt, and Lewis numbers: $Pr \equiv c_p \mu/\lambda$; $Sc \equiv \mu/(\rho D)$; and $Le \equiv Sc/Pr$.

Steady-state flow will be assumed. There will be no dependence throughout the two free streams of the u and v velocity components, the rates of normal strain, or the scalar properties on the x or z coordinates. Consequently, the shear layer will have velocity components u and v depending only on y; $w = \kappa z$ where κ depends only on y. Here, the variable κ becomes the constant strain rate S in the free stream as $y \to \infty$. If the densities in the two free streams differ, κ approaches a modified constant as $y \to -\infty$. Furthermore, $u \to U > 0$ as $y \to +\infty$ and $u \to -U$ as $y \to -\infty$. The velocity component $v \to -Sy$ as $y \to +\infty$ and $v \to -Sy$ as $y \to -\infty$. The y-coordinate will be set so that $v(0) = 0$. From the steady-state continuity equation, it follows that

$$f \equiv \int_0^y \rho(y')\kappa(y')dy' = -\rho(y)v(y) \tag{6}$$

Using a classical approach for variable-density shear layers, the y coordinate can be conveniently replaced by $\eta \equiv \int_0^y \rho(y')dy'$. Also, the product $\rho\mu$ may be considered to be constant with y, retaining the value $\rho_\infty \mu_\infty$. Note that now $\kappa = df/d\eta$.

Under the prescribed constraints, many terms in the momentum equation become identically equal to zero. The three momentum equations can be given in the following convenient albeit non-conventional forms. For the x-momentum equation, the pressure is constant in the x-direction and, given the free-stream conditions, a solution exists with $\tau_{xx} = 0, \tau_{xz} = 0, \partial u/\partial x = 0$, and $\partial u/\partial z = 0$. Thus,

$$\rho_\infty \mu_\infty \frac{\partial^2 u}{\partial \eta^2} + f \frac{\partial u}{\partial \eta} = 0 \tag{7}$$

For the y-momentum equation, a solution is found with v independent of x and z. So, τ_{yx} is independent of x and τ_{yz} is independent of z. Specifically, we have

$$\frac{\partial p}{\partial \eta} = \frac{4}{3}\rho_\infty \mu_\infty \frac{\partial^2 v}{\partial \eta^2} + f \frac{\partial v}{\partial \eta} - \frac{2}{3}\frac{\partial(\mu\kappa)}{\partial \eta} + \mu \frac{\partial \kappa}{\partial \eta} \tag{8}$$

The z-momentum equation has w independent of x and linear in z, $\tau_{zx} = 0$, and $\partial \tau_{zz}/\partial z = 0$. Thereby, after each remaining term is divided by z, we obtain an equation for κ, the local rate of normal strain.

$$\frac{1}{z}\frac{\partial p}{\partial z} = \rho\left[\rho_\infty \mu_\infty \frac{\partial^2 \kappa}{\partial \eta^2} + f \frac{\partial \kappa}{\partial \eta} - \kappa^2 \right] \tag{9}$$

The right side of the y- and z-momentum equations are functions of η only. Thus, by differentiation of the y momentum equation, we realize that

$$\frac{\partial^2 p}{\partial \eta \partial z} = 0 \tag{10}$$

It follows that the derivative of the right side of the z-momentum equation with respect to η produces zero, implying that the right side equals a constant. Matching the right side to values at $\eta = +\infty$, that constant is found to be $-\rho_\infty \kappa_\infty^2$. Consequently, we obtain three ordinary differential equations:

$$\rho_\infty \mu_\infty \frac{d^2 u}{d\eta^2} + f \frac{du}{d\eta} = 0 \tag{11}$$

$$\frac{dp}{d\eta} = \frac{4}{3}\rho_\infty \mu_\infty \frac{d^2 v}{d\eta^2} + f\frac{dv}{d\eta} - \frac{2}{3}\frac{d(\mu\kappa)}{d\eta} + \mu\frac{d\kappa}{d\eta} \tag{12}$$

$$\rho_\infty \mu_\infty \frac{d^2 \kappa}{d\eta^2} + f\frac{d\kappa}{d\eta} - \kappa^2 + \frac{\rho_\infty \kappa_\infty^2}{\rho} = 0 \tag{13}$$

Given that $\kappa = df/d\eta$, Eq. (13) can be recast as a third-order ordinary differential equation for f. However, in order to obtain numerical solutions, it is preferred to keep the second-order equation for κ and the first-order equation for f. Then, a better match occurs with the two-point-boundary-value-problem nature for other variables. Also, κ has important physical meaning as the rate of normal strain; thereby, tracking it has value.

With proper use of the boundary conditions and coupling with the scalar equation solutions to determine ρ, Eq. (13) can be first solved for κ; then, f and v can be determined from integration with Eq. (6); this allows integration of Eqs. (11) and (12) to determine u and p.

Eqs. (4) and (5) can also be reduced to ordinary differential equations under the constraints here. In addition, we consider $Le = 1$ and Pr to be constant. The resulting equations are

$$\frac{1}{Pr}\frac{d^2 h}{d\eta^2} + f\frac{dh}{d\eta} + \Sigma_{m=1}^{N} h_{f,m}\dot{\omega}_m = 0 \tag{14}$$

$$\frac{1}{Pr}\frac{d^2 Y_m}{d\eta^2} + f\frac{dY_m}{d\eta} + \dot{\omega}_m = 0 \ , \quad m = 1, 2, \ldots, N \tag{15}$$

A conserved scalar $\bar{h}(\eta)$ can be formed, summing both thermal energy and chemical energy, when kinetic energy and viscous dissipation can be neglected: $\bar{h} = h + \Sigma_{m=1}^{N} h_{f,m} Y_m$. Other conserved scalars can be created. Mixture fraction is a popular choice, except that it serves no use for premixed flames and is bypassed here.

In the remainder of this article, the non-dimensional forms of the above equations are considered. u is normalized by U; v and w are normalized by $[S\mu_\infty/\rho_\infty]^{1/2}$ where $S = \kappa_\infty$ is the magnitude of the imposed normal compressive strain in the negative y direction at large values of y.

The variables t, x_i, ρ, h, p, and $\dot{\omega}_m$, and properties $\mu, \lambda/c_p$, and D are normalized respectively by $(S)^{-1}, [\mu_\infty/(\rho_\infty S)]^{1/2}$, ρ_∞, h_∞, $S\mu_\infty$, S, μ_∞, μ_∞, and μ_∞/ρ_∞. Note that the reference length $[\mu_\infty/(\rho_\infty S)]^{1/2}$ is the estimate for the magnitude of the viscous-layer thickness. We can assume that for thermodynamic relations, pressure can be considered uniform through the field because of low values of Mach number. Thereby, the non-dimensional relation is $h = 1/\rho$. Now, in nondimensional form, Eqs. (14) and

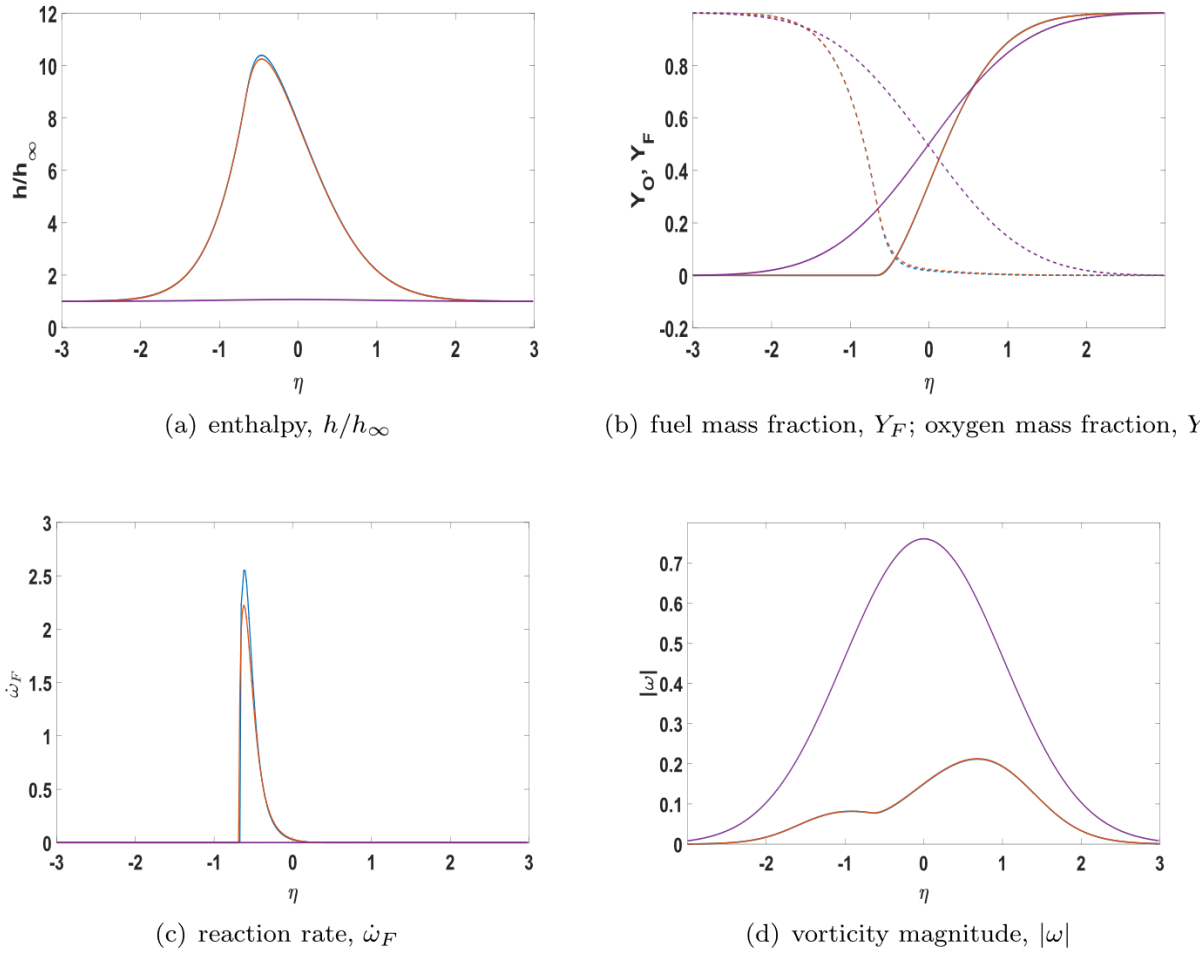

(a) enthalpy, h/h_∞ (b) fuel mass fraction, Y_F; oxygen mass fraction, Y_O

(c) reaction rate, $\dot{\omega}_F$ (d) vorticity magnitude, $|\omega|$

Fig. 2. Diffusion flame with varying Damköhler number. blue, $K = 0.250$; red, $K = 0.204$; purple, $K = 0.203$. Dashed lines for oxygen and solid lines for fuel. (For interpretation of the references to colour in this figure legend, the reader is referred to the web version of this article.)

(15) remain identical while Eqs. (11) and (13) change modestly to the forms

$$\frac{d^2u}{d\eta^2} + f\frac{du}{d\eta} = 0 \tag{16}$$

$$\frac{d^2\kappa}{d\eta^2} + f\frac{d\kappa}{d\eta} - \kappa^2 + h = 0 \tag{17}$$

Eq. (6) may be written in non-dimensional form as

$$f(\eta) = \int_0^\eta \kappa(\eta')d\eta' = -\rho(\eta)v(\eta) \tag{18}$$

The boundary conditions in non-dimensional form are

$$\begin{aligned}
&u(\infty) = 1 \ ; \ u(-\infty) = -1; \ ; \\
&\kappa(\infty) = 1 \ ; \ \kappa(-\infty) = \sqrt{h_{-\infty}}; \ ; \\
&h(\infty) = 1 \ ; \ h(-\infty) = \frac{1}{\rho_{-\infty}} \ ; \\
&Y_m(\infty) = Y_{m,\infty} \ ; \ Y_m(-\infty) = Y_{m,-\infty} \ ; \\
&\tilde{h}(\infty) = 1 + \Sigma_{m=1}^N h_{f,m}Y_{m,\infty} \ ; \ \tilde{h}(-\infty) = h_{-\infty} + \Sigma_{m=1}^N h_{f,m}Y_{m,-\infty}
\end{aligned} \tag{19}$$

Eq. (11) can be replaced with an integral form.

$$I(\eta) \equiv \int_0^\eta f(\eta')d\eta'$$

$$u(\eta) = 2\frac{\int_{-\infty}^\eta e^{-I(\eta')}d\eta'}{\int_{-\infty}^{+\infty} e^{-I(\eta)}d\eta} - 1 \tag{20}$$

Note that with variable density $I(\eta)$ is no longer an even function and therefore the inflection point for the u curve will generally not be at $y = 0$, i.e., at $\eta = 0$.

An exact solution of the variable-density Navier-Stokes equation for multicomponent, reacting flow has been obtained for the case where the w velocity component is linear in z and all velocity components are independent of x. If the w behavior deviates from linear, the solution may be regarded as an approximation with the neglect of terms of $O(z^2)$. First, simultaneous solution of Eqs. (14), (15), (17) coupled with the relation given by Eq. (6) is needed; then, it can be followed by use of Eq. (20). Unlike the incompressible counterflow, a viscous layer exists with the normal strains and normal viscous stresses varying through the layer due to varying density and viscosity. The dimensional forms of the scalar properties and the two transverse velocity components in the layer depend only on the imposed normal strain and the scalar free-stream conditions. They do not depend on shear strain or vorticity. Only the streamwise component of velocity through the layer will depend on shear strain and thus on vorticity.

The vorticity in this configuration is given as

$$\begin{aligned}
\omega &= -\frac{du}{dy} = -\rho\frac{du}{d\eta} = -\frac{1}{h}\frac{du}{d\eta} \\
\omega(\eta) &= -\frac{2}{h}\frac{e^{-I(\eta)}}{\int_{-\infty}^{+\infty} e^{-I(\eta)}d\eta}
\end{aligned} \tag{21}$$

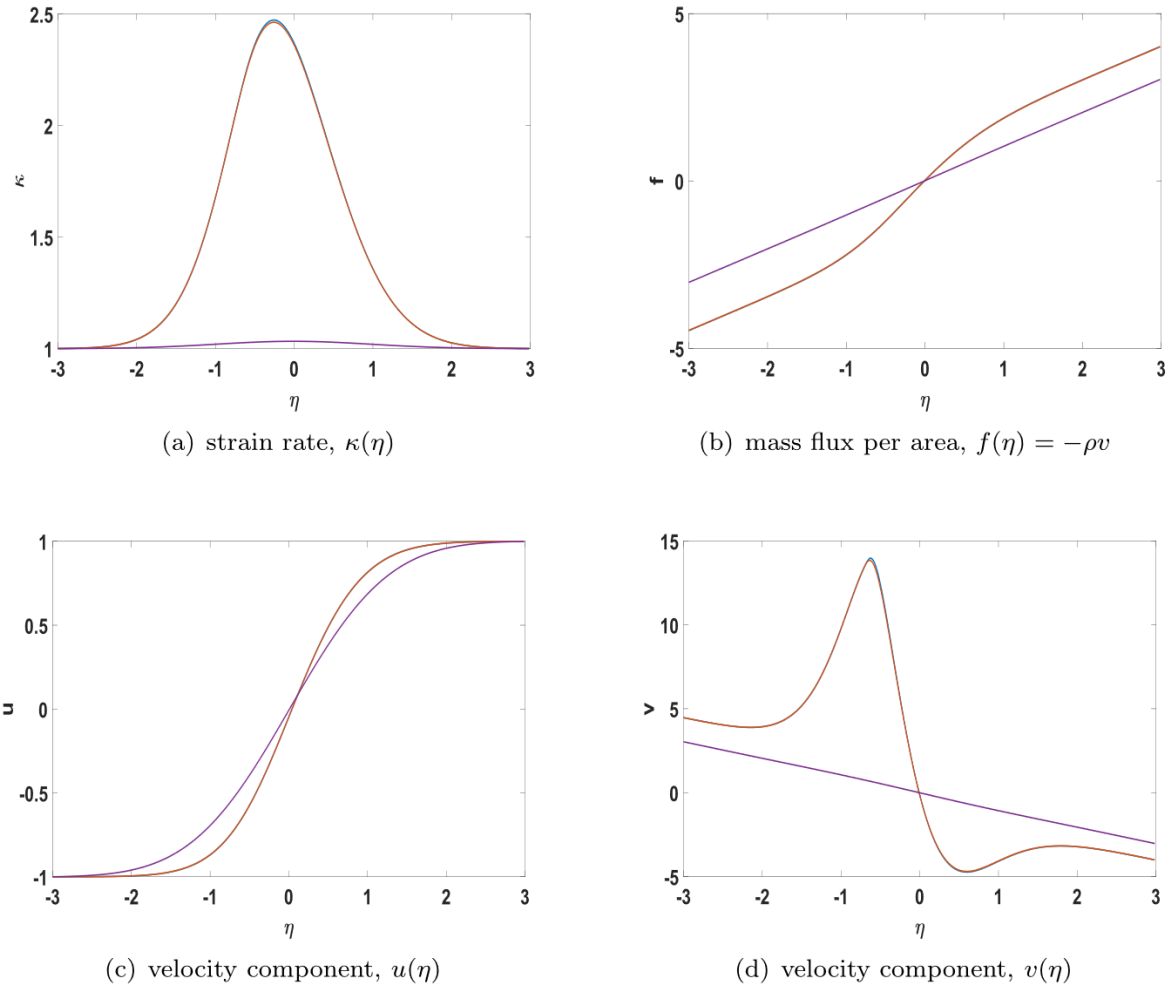

(a) strain rate, $\kappa(\eta)$ (b) mass flux per area, $f(\eta) = -\rho v$

(c) velocity component, $u(\eta)$ (d) velocity component, $v(\eta)$

Fig. 3. Diffusion flame with varying Damköhler number. blue, $K = 0.250$; red, $K = 0.204$; purple, $K = 0.203$. (For interpretation of the references to colour in this figure legend, the reader is referred to the web version of this article.)

2.2. Chemical kinetics model

The above equations can be readily applied for diffusion-flame, multi-branched-flame, and premixed-flame counterflows and partially-premixed-flame counterflows as will be exemplified in the following section. In related studies, the generality has been shown [12,16]. We will consider propane-oxygen flows with one-step kinetics. The intention is to consider detailed kinetics in the future since it is allowed by this analytical frmework. Results are expected to be qualitatively more general, applying to situations with more detailed kinetics and to other hydrocarbon /oxygen-or-air combination. The kinetics given by Westbrook and Dryer [38] are used. Y_F, Y_O, ν_S, and Q are fuel mass fraction, oxygen mass fraction, stoichiometric mass ratio, and chemical energy per unit mass of fuel, respectively.

In non-dimensional terms, the reaction rate for propane is given by

$$\dot{\omega}_F = -\frac{Da}{h^{0.75}} Y_F^{0.1} Y_O^{1.65} e^{-50.237/h} \tag{22}$$

where the Damköhler number Da is defined as

$$Da = \frac{A\rho_\infty^{0.75}}{\kappa_\infty} \tag{23}$$

with $A^* = 4.79 \times 10^8 (kg/m^3)^{-0.75}/s$ and density and strain rate given in dimensional terms. The value in the exponent of Eq. (22) implies that the reference temperature, which is the inflow temperature at $y = \infty$ has been set at $300K$. For convenience, a reference Damköhler number Da_{ref} is used with 10 kg/m^3 and 10,000/s chosen as reference values for density and strain rate, respectively. The reference value for density implies an elevated pressure. The strain-rate reference value is in the middle of an interesting range for this chemical reaction. Furthermore, $Da \equiv KDa_{ref}$; thus, variation of K is used to study the effect of Da. Accordingly,

$$Da_{ref} \equiv \frac{\tilde{A}(10kg/m^3)^{0.75}}{(10^4/s)} = 2.693 \times 10^5 \ ;$$
$$K \equiv \left[\frac{\rho_\infty^*}{10kg/m^3}\right]^{0.75} \frac{10^4/s}{S_1^* + S_2^*} \tag{24}$$

Clearly, there is no need to set pressure (or its proxy, density) and the strain rate separately for a one-step reaction. For propane and oxygen, the mass stoichiometric ratio $\nu = 0.275$. The non-dimensional parameter K increases (decreases) as the strain rate decreases (increases) and/ or the pressure increases (decreases). $K = 1$ is our reference case and the range covered includes $O(10^{-1}) \le K \le O(10^2)$, allowing for the needed variation in strain rate and pressure to sustain premixed flamelets, diffusion flamelets, and multi-branched flamelets. Da can be viewed as a ratio of chemical reaction rate to strain rate or, since residence time

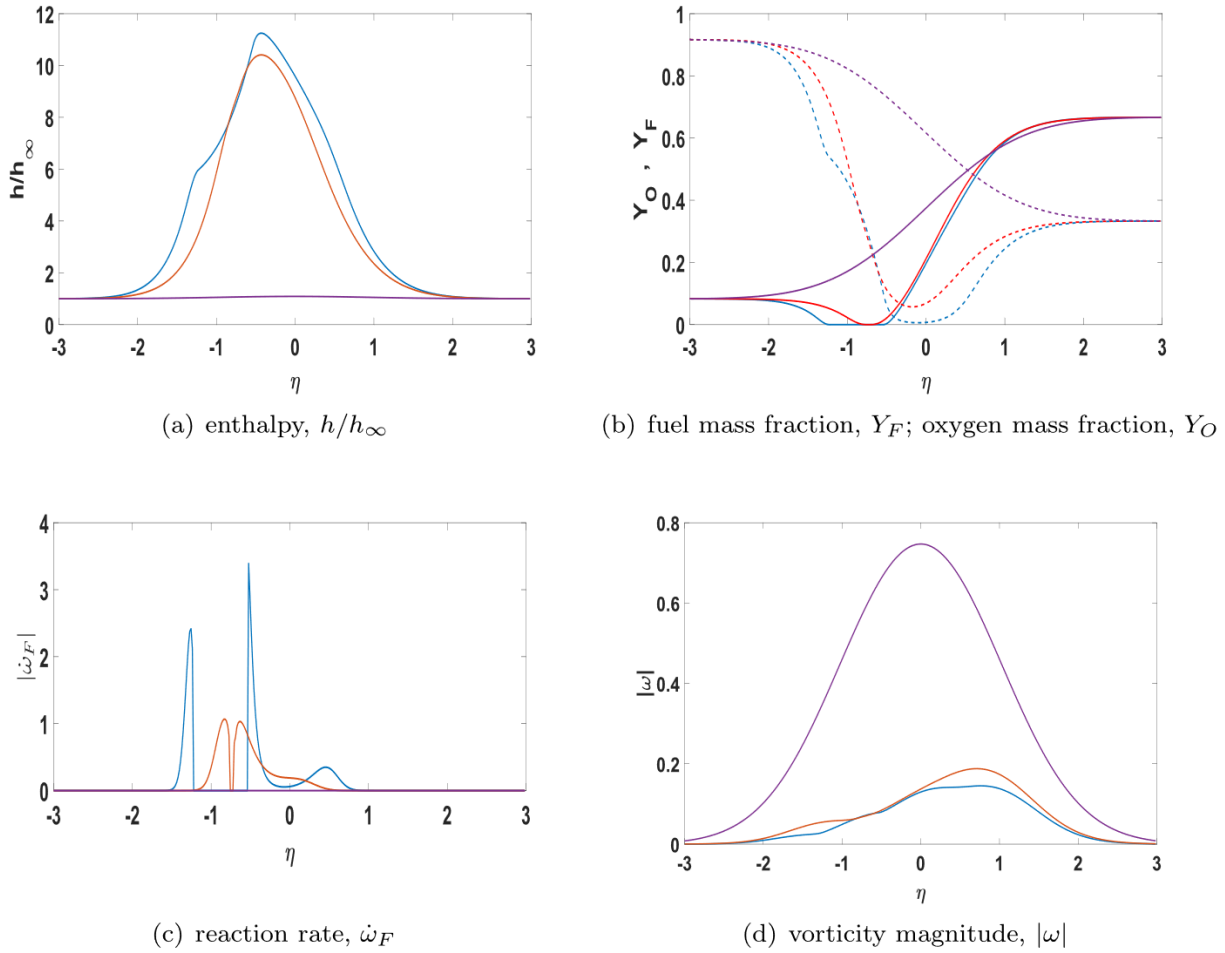

(a) enthalpy, h/h_∞

(b) fuel mass fraction, Y_F; oxygen mass fraction, Y_O

(c) reaction rate, $\dot{\omega}_F$

(d) vorticity magnitude, $|\omega|$

Fig. 4. Multi-flame structure with varying Damköhler number. blue, $K = 1.000$; red, $K = 0.109$; purple, $K = 0.108$. Dashed lines for oxygen and solid lines for fuel. (For interpretation of the references to colour in this figure legend, the reader is referred to the web version of this article.)

is the reciprocal of strain rate, a ratio of residence time to chemical time.

For case of one-step kinetics with $Le = 1$ and negligible viscous dissipation, the Shvab-Zel'dovich variables, $\alpha \equiv Y_F - \nu_S Y_O$ and $\beta \equiv h + \nu_S Y_O Q$ become conserved scalars. For steady-state and time-averaged flows, these conserved scalars vary monotonically across a flow field.

3. Results and discussion

The system of ordinary differential equations is solved numerically using a relaxation method and central differences. Solution over the range $-5 \leq \eta \leq 5$ provides adequate fittings to the asymptotic behaviors. The parameters that can be varied are K, Pr, and the boundary conditions at $\eta = \infty$ and $\eta = -\infty$. Here, calculations have $Pr = 1$ with emphasis on the effect of variations in K (i.e., pressure and strain rate) and the inflowing mixture composition.

In the following three subsections, the three possible flame configurations are analyzed: diffusion flames, multi-branched flames, and premixed flames.

3.1. Diffusion flamelet calculations

Now, we treat a situation with a sole diffusion flame in the flamelet structure. Figures 2 and 3 show the influence of Da on the flamelet stability near the extinction limit. The blue and red curves represent K values of 0.250 and 0.204, respectively. A strong flame is obtained with very modest differences in the results over this range of K. The slight decrease of K to the value of 0.203 results in extinction as indicated by the purple curve. The flame occurs in the inflowing oxygen stream at negative values of y and η. While ρv monotonically decreases with increasing y or η, the velocity v is not monotonic. Thus, the normal strain rate dv/dy changes sign when the flame produces a region of low density. Accordingly, a maximum value of the normal strain rate κ occurs in the flame zone. The extinguished flame case actually shows a higher maximum value of vorticity $\omega = -du/dy$ in the shear layer. The integral of vorticity across the shear layer in y-space has the same value of $-\Delta u = -u_\infty + u_{-\infty} = -2$ in all cases. The lower density in the flame cases causes a larger shear layer width Δy. Realize that the plot of Fig. 2d is deceptive on that point because η rather than y is used. Note further that the dependence on density (and thereby temperature or enthalpy) causes two local maxima in the vorticity to appear in the plot.

The interesting and consequential result here which differs from other flamelet situations is that vorticity and shear strain do not affect the scalar profiles, transport rates, or burning rates. On the contrary, the scalar behavior does affect the vorticity. In other flamelet configurations [24,25], the vorticity could affect extinction and flammability limits.

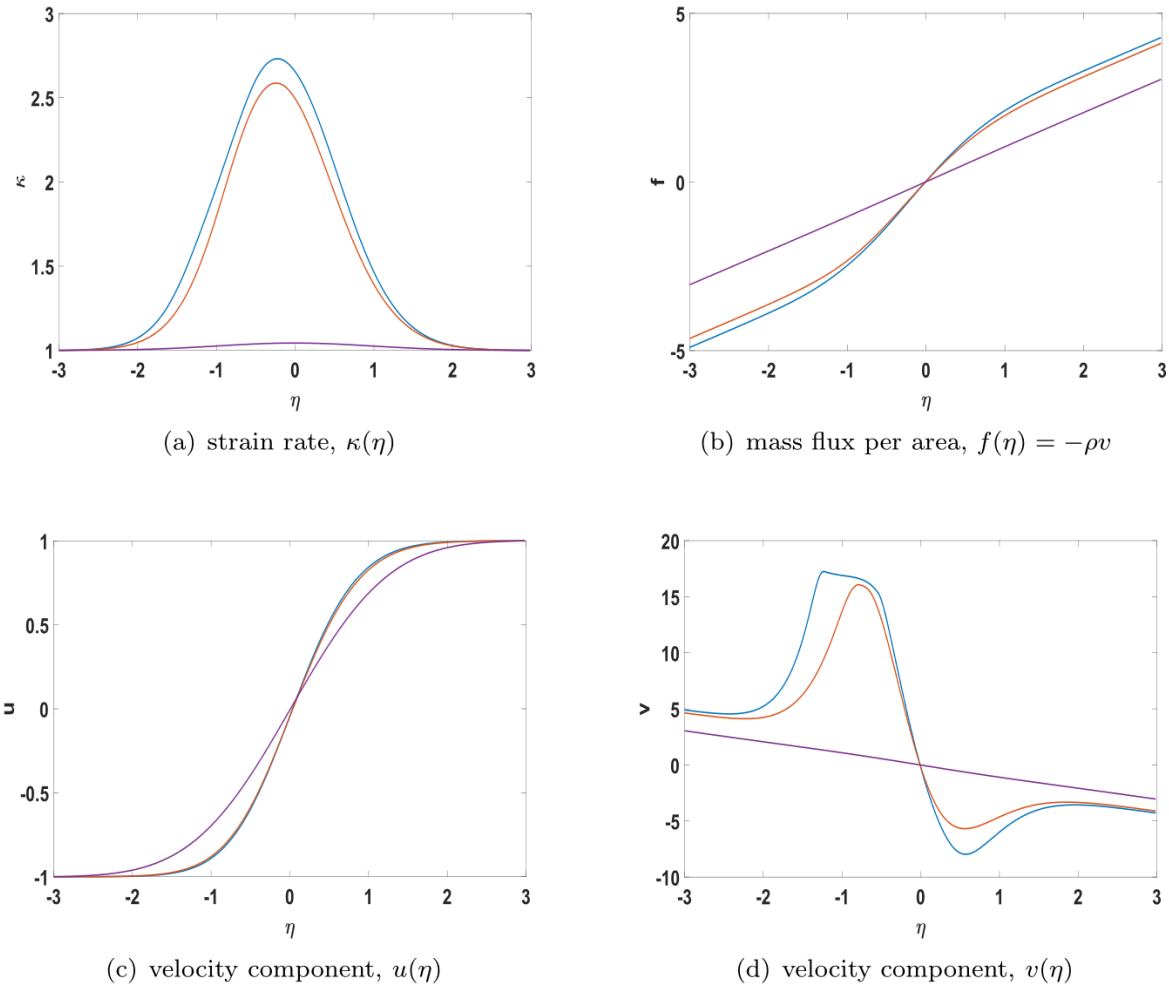

(a) strain rate, $\kappa(\eta)$ (b) mass flux per area, $f(\eta) = -\rho v$

(c) velocity component, $u(\eta)$ (d) velocity component, $v(\eta)$

Fig. 5. Multi-flame structure with varying Damköhler number. blue, $K = 1.000$; red, $K = 0.109$; purple, $K = 0.108$. (For interpretation of the references to colour in this figure legend, the reader is referred to the web version of this article.)

3.2. Multi-flamelet calculations

The counterflowing streams involve a fuel-lean mixture, with $Y_O = 11/12, Y_F = 1/12$, flowing inward from $y = -\infty$ and a fuel-rich mixture, with $Y_F = 2/3, Y_O = 1/3$, flowing inward from $y = \infty$. For $K \geq 0.109$, three flames are seen in Figs. 4 and 5; a fuel-lean premixed flame, a diffusion flame, and a fuel-rich premixed flame. For $K \leq 0.108$, the flames are extinct. An important feature is that the premixed flames require a significantly larger value of *Da* (larger reaction rate and/ or smaller strain rate) compared to the diffusion flame to maintain their strength. As K increases, the diffusion flame modestly strengthens but significant strengthening of the two premixed flames are seen. In the wide range of K shown here, the two premixed flames are driven by heat transport from the diffusion flame. So, in the cases described here, the premixed flames are not independent but rather rely on multi-branched flame structure to exist. This finding is consistent with the prior results [24,25,39]. The premixed flames strengthen as K increases with the fuel-lean flame shower greater strength and a larger degree of independence from the diffusion flame. Specifically, with increasing *Da*, the premixed flames move away from the diffusion flame towards positions with higher inflow velocity and lower heat flux from the downstream diffusion flame.

Qualitatively, the same effects of variable density and temperature on the velocity and vorticity are seen in this case as was seen for the diffusion flame. The one-way coupling between scalar behavior and vorticity appears as well.

3.3. Premixed-flame calculations

In our analysis for a premixed flame, the incoming stream from $y = \infty$ is a stiohiometric mixture that is 43.5 percent oxygen and 12 percent propane with the remainder an inert gas. Only an inert gas inflows from $y = -\infty$. For a premixed flame to survive independently in the counterflow, an increase in the value of D (and therefore of K) by roughly two orders of magnitude is required compared to the multi-branched flame. See Figs. 6 and 7 with comparison to the earlier figures. There is a value of K between 20 and 21 where extinction occurs sharply. As K increases about that value the peak values of enthalpy and temperature remain constant; however, the premixed flame speed increases and the flame position changes such that the inflow velocity is higher. The peak value of vorticity associated with the shear flow is higher after extinction while the shear layer is thinner. Again, the vorticity has no effect on the scalar profiles but it is affected by enthalpy.

Once *Da* is high enough for a flame to exist, $u(\eta)$ does not change significantly with *Da* while $h(\eta)$ and therefore $\rho(\eta)$ do vary with *Da*. Since $u(\eta)$ does not vary, $du/d\eta$ will not vary. This implies that the change of u, namely Δu, over a given change in mass per unit area, $\Delta\eta = \rho\Delta y$, remains unchanged with changing

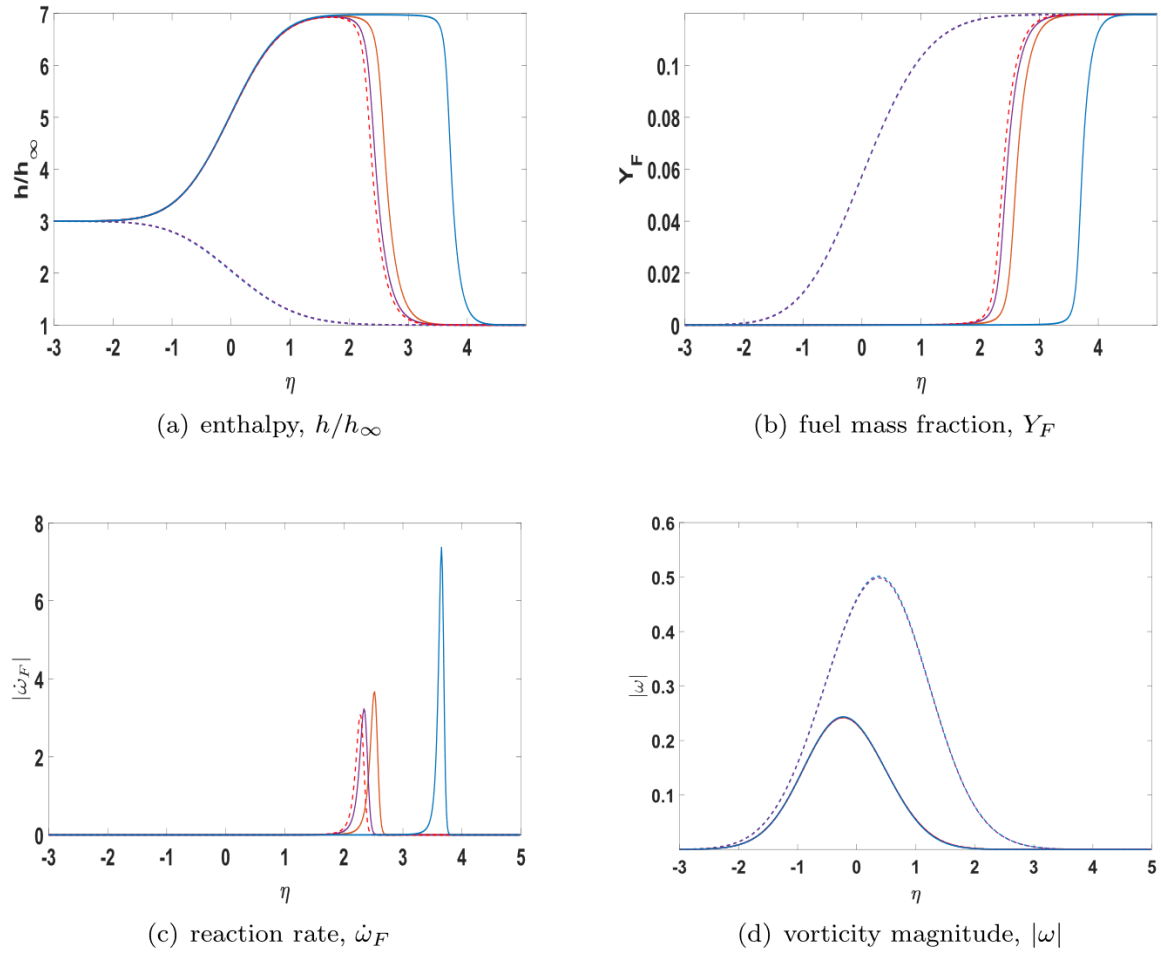

Fig. 6. Premixed flame with varying Damköhler number. Blue, $K = 50.0$; red, $K = 25.0$; purple, $K = 22.0$; dash red, $K = 21.0$; dash purple, $K = 20.0$. (For interpretation of the references to colour in this figure legend, the reader is referred to the web version of this article.)

Da and associated changes in the profiles of h and ρ. We would expect that since $du/d\eta$ does not change with η but ρ does change, the vorticity $\omega = -du/dy = -\rho du/d\eta$ must change as *Da* is varied. However, Fig. 6d shows no change. The explanation is that Fig. 6a shows the deviation in h values with changing *Da* occurs for $\eta > 1$ where little variation in u occurs as η changes resulting in small values of vorticity therefore in that η domain. The significant magnitudes of vorticity appear in regions where density and enthalpy do not vary as *Da* varies. Again, like the cases in the earlier subsections, the integral of the vorticity across the layer again depends only on the difference between the two free-stream velocities and thereby is independent of flame behavior. However, the density variation affects the layer width and the distribution of the vorticity.

4. Concluding remarks

Recently, several new flamelet models have been constructed for sub-grid modelling of turbulent combustion in LES and RANS analysis [24,25]. Here, a third related flamelet model is developed based on a stretched-vortex-layer configuration. These new flamelet models present certain advanced features: (i) nonpremixed flames, premixed flames, or multi-branched flame structures are allowed to appear naturally without prescription; (ii) the impacts of shear strain and vorticity on the flames are determined; (iii) the applied sub-grid strain rates and vorticity may be directly related to the resolved-scale strain rates and vorticity without the use of a contrived progress variable; and (iv) variable density is allowed in the flamelet. These features allow vital physics that is missed by current irrotational, constant-density flamelet models that assume a priori a nonpremixed- or premixed-flame structure and do not connect to shear strain or vorticity [2,7,8]. Sirignano [24] considers a rotational flamelet with uniform vorticity over the small flamelet domain; the three-dimensional counterflow has one compressive-normal-strain direction aligned with scalar gradients and two extensional-normal-strain directions. Sirignano [25] considers a stretched vortex tube with inward swirl created by two compressive-strain directions and the extensional direction aligned with the vorticity vector. Now, a model is introduced where shear strain is explicitly represented in the x, y plane creating a vortex layer with counterflow in the y, z plane producing vortex stretching. Given that experiments [37] and direct numerical simulation [21] both indicate that a range of vortical structures will co-exist in a turbulent flow, more than one type of flamelet model is needed. It does remain however to develop a methodology for choosing the best flamelet model for application at a specific point in space and time for a domain with turbulent combustion.

The analytical frameworks allow for multi-step, detailed kinetics although the calculations are limited to one-step propane-oxygen kinetics. The quasi-steady assumption commonly used in previous flamelet models is maintained here for the stretched-vortex-layer flamelet. Premixed flames can only exist with orders-of-magnitude larger values of *Da* compared to diffusion flamelets or multibranched flames. So, premixed flames will be less likely to

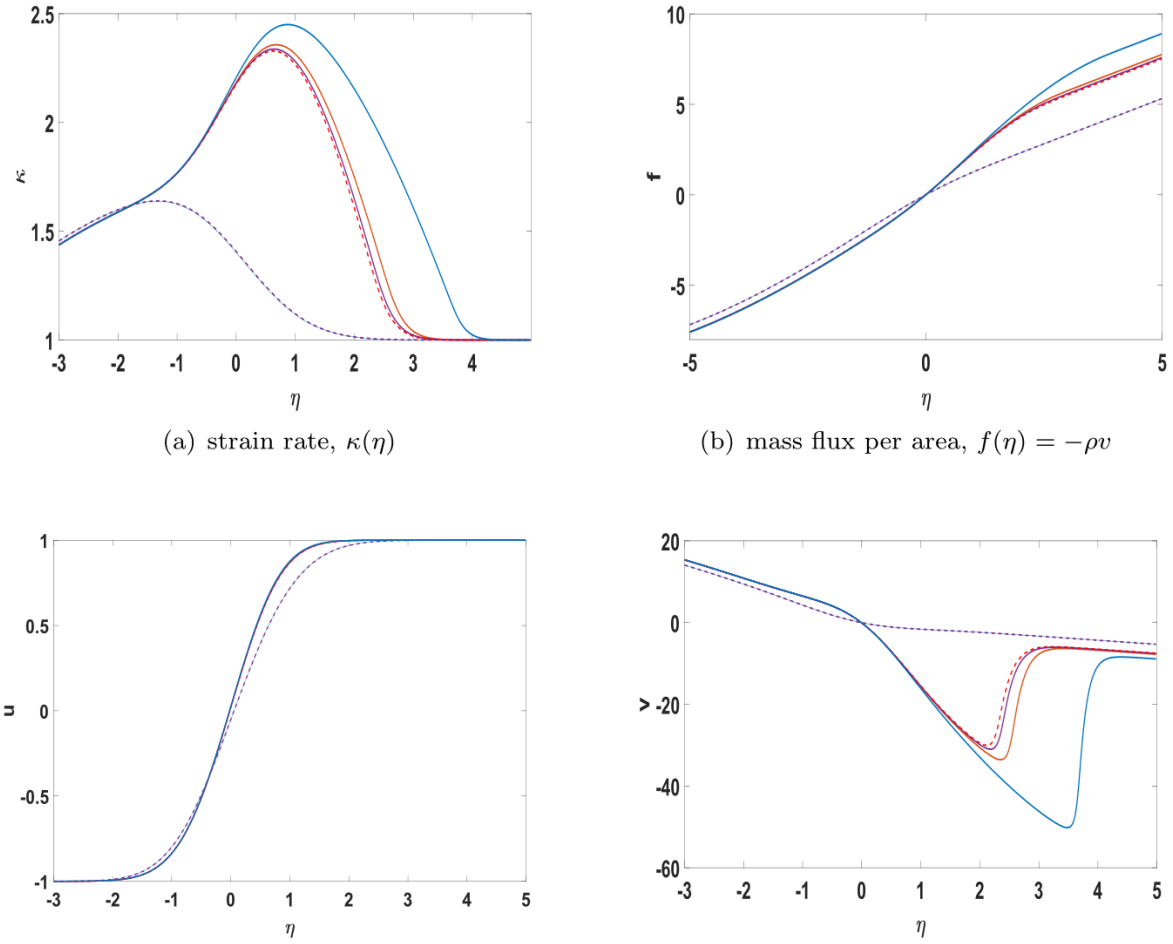

(a) strain rate, $\kappa(\eta)$ (b) mass flux per area, $f(\eta) = -\rho v$

(c) velocity component, $u(\eta)$ (d) velocity component, $v(\eta)$

Fig. 7. Premixed flame with varying Damköhler number. Blue, $K = 50.0$; red, $K = 25.0$; purple, $K = 22.0$; dash red, $K = 21.0$; dash purple, $K = 20.0$. (For interpretation of the references to colour in this figure legend, the reader is referred to the web version of this article.)

survive extinction in a turbulent situation with high strain rates. The partially premixed flames in a multi-branched flame structure are driven by heat flux from the diffusion flame; thereby, they survive at lower values of *Da*.

In the rotational flamelet and the stretched-vortex-tube three-dimensional models, the imposed vorticity had consequence on the scalar fields and the burning rate through the centrifugal acceleration. However, here, the vortex-layer model is asymptotically two-dimensional with no centrifugal effect, and a resulting one-way coupling between the scalar field and the vorticity; vorticity does not affect scalar profiles while the scalars can have some influence on vorticity.

In the future, multi-step kinetics should be utilized with the new flamelet model. It would be interesting to explore the unstable branch of combustion on the plot of peak temperature or burning rate versus scalar dissipation rate. In a dynamic situation, the unstable branch could have impact.

Declaration of Competing Interest

The authors declare that they have no known competing financial interests or personal relationships that could have appeared to influence the work reported in this paper.

Acknowledgements

The effort was supported by AFOSR through Award FA9550-18-1-0392 managed by Dr. Mitat Birkan.

References

[1] F.A. Williams, Recent advances in theoretical descriptions of turbulent diffusion flames, in: S.N.B. Murthy (Ed.), Turbulent Mixing in Nonreactive and Reactive Flows, Springer (1975), pp. 189–208.
[2] A. Linan, The asymptotic structure of counterflow diffusion flames for large activation energies, Acta Astonautica 1 (1974) 1007–1039.
[3] F.E. Marble, Growth of a diffusion flame in the field of a vortex, Recent Advances in the Aerospace Sciences, Plenum Press, New York (1985), pp. 395–413.
[4] A.R. Karagozian, F.E. Marble, Study of a diffusion flame in a stretched vortex, Combust. Sci. Technol. 45 (1986) 65–84.
[5] B.M. Cetegen, W.A. Sirignano, Study of molecular mixing and a finite rate chemical reaction in a mixing layer, Proceedings of Twenty-Second Symposium (International) on Combustion, Combustion Institute, Pittsburgh (1988), pp. 489–494.
[6] B.M. Cetegen, W.A. Sirignano, Study of mixing and reaction in the field of a vortex, Combust. Sci. Technol. 72 (1990) 157–181.
[7] N. Peters, Turbulent combustion, first ed., Cambridge University Press, Cambridge, UK, 2000.
[8] C. Pierce, P. Moin, Progress-variable approach for large-eddy simulation of non-premixed turbulent combustion, J. Fluid Mech. 504 (2004) 73–97.
[9] F.A. Williams, Progress in knowledge of flamelet structure and extinction, Prog. Energy Combust. Sci. 26 (2000) 657–682.

[10] J.A. van Oijen, A. Donini, R. Bastiaans, J. ten Thije Boonkkamp, L. de Goey, State-of-the-art in premixed combustion modeling using flamelet generated manifolds, Prog. Energy Combust. Sci. 57 (2016) 30–74.
[11] M.E. Mueller, Physically-derived reduced-order manifold-based modeling for multi-modal turbulent combustion, Combust. Flame 214 (2020) 287–305.
[12] W.A. Sirignano, Combustion with multiple flames under high strain rates, Combust. Sci. Technol. 192 (2021) 1173–1202.
[13] A. Hamins, H. Thridandam, K. Seshadri, Structure and extinction of a counterflow partially premixed, diffusion flame, Chem. Eng. Sci. 40 (1985) 2027–2038.
[14] P. Rajamanickam, W. Coenen, A.L. Sanchez, F.A. Williams, Influences of stoichiometry on steadily propagating triple flames in counterflows, Proc. Combust. Inst. 37 (2019) 1971–1977.
[15] W.A. Sirignano, Mixing and combustion in a laminar shear layer with imposed counterflow, J. Fluid Mech. 908 (2021) 1–33A35.
[16] W.A. Sirignano, Counterflow and wall stagnation flow with three-dimensional strain, Phys. Fluids 31 (2019) 053605, doi:10.1063/1.5096472.
[17] C.-F. López-Cámara, A. Jordà Juanós, W.A. Sirignano, Strain rate and pressure effects on multi-branched counterflow flames, Combust. Flame 221 (2020) 256–269.
[18] W. Ramaekers, J.A. van Oijen, L. de Goey, A priori testing of flamelet generated manifolds for turbulent partially premixed methane/air flames, Flow Turbul. Combust. 84 (2010) 439–458.
[19] W.T. Ashurst, A.R. Kerstein, R.M. Kerr, C.H. Gibson, Alignment of vorticity and scalar gradient with strain rate in simulated Navier-Stokes turbulence, Physics of Fluids 30 (1987) 2343–2352.
[20] K.K. Nomura, S.E. Elghobashi, Mixing characteristics of an inhomogeneous scalar in isotropic and homogeneous sheared turbulence, Phys. Fluids A 4 (1992) 606–625.
[21] K.K. Nomura, S.E. Elghobashi, The structure of inhomogeneous turbulence scalar in variable density nonpremixed flames, Theor. Comput. Fluid Dyn. 5 (1993) 153–175.
[22] O.N. Boratav, S.E. Elghobashi, R. Zhong, On the alignment of the a-strain and vorticity in turbulent nonpremixed flames, Phys. Fluids 8 (1996) 2251–2253.
[23] O.N. Boratav, S.E. Elghobashi, R. Zhong, On the alignment of strain, vorticity and scalar gradient in turbulent, buoyant, nonpremixed flames, Phys. Fluids 10 (1998) 2260–2267.
[24] W.A. Sirignano, Three-dimensional, rotational flamelet closure model with two-way coupling, J. Fluid Mech. (2022) arXiv:2111.11365. in press.
[25] W.A. Sirignano, Inward swirling flamelet model, in journal review (2022) arXiv:2203.06284.
[26] J.M. Burgers, Unpublished lectures on turbulence, California Institute of Technology (1951).
[27] G.K. Batchelor, An introduction to fluid dynamics, Cambridge University Press, Cambridge, UK, 1967.
[28] A.C. Robinson, P.G. Saffman, Stability and structure of stretched vortices, Stud. Appl. Math. (1984).
[29] J.L. Palafoutas, W.A. Sirignano, Reacting and non-reacting, three-dimensional shear layers with spanwise stretching, in journal review (2022) arXiv:2206.05587.
[30] J.M. Burgers, A mathematical model illustrating the theory of turbulence, Adv. Appl. Mech. 1 (1948) 171–199.
[31] N. Rott, On the viscous core of a line vortex, Z. Angew. Math. Phys. IXb (1958) 543–553.
[32] J.C. Neu, The dynamics of stretched vortices, J. Fluid Mech. 143 (1984) 253–276.
[33] P.G. Saffman, Vortex dynamics, Cambridge University Press, Cambridge, UK, 1992.
[34] G.M. Corcos, F.S. Sherman, The mixing layer: deterministic models of a turbulent flow. Part 1. Introduction and the two-dimensional flow, J. Fluid Mech. 139 (1984) 29–65.
[35] G.M. Corcos, S.J. Lin, The mixing layer: deterministic models of a turbulent flow. Part 2. The origin of the three-dimensional motion, J. Fluid Mech. 139 (1984) 67–95.
[36] S.J. Lin, G.M. Corcos, The mixing layer: deterministic models of a turbulent flow. Part 3. The effect of plane strain on the dynamics of streamwise vortices, J. Fluid Mech. 141 (1984) 139–178.
[37] K.A. Buch, W.J.A. Dahm, Experimental study of fine-scale structure of conserved scalar mixing in turbulent shear flows. Part 2. Sc $\approx$ 1, J. Fluid Mech. 364 (1998) 1–29.
[38] C.K. Westbrook, F.L. Dryer, Chemical kinetic modeling of hydrocarbon combustion, Prog. Energy Combust. Sci. (10) (1984) 1–57.
[39] W.A. Sirignano, Diffusion-controlled premixed flames, Combust. Theory Modell. 25 (2021). Invited paper for special issue in honor of Professor Moshe Matalon.